







Electrophysiology and 3D-imaging reveal properties of human intracardiac neurons and increased excitability with atrial fibrillation

J. L. Ashton^{1,2} , B. Prince^{1,2}, G. Sands³ , L. Argent^{1,2} , M. Anderson⁴, J. E. G. Smith^{1,2} , A. Tedoldi^{1,2} , A. Ahmad^{1,2}, D. Baddeley³, A. G. Pereira¹ , N. Lever^{2,3,5}, T. Ramanathan^{2,4}, B. H. Smail^{2,3} and Johanna M. Montgomery^{1,2}

¹Department of Physiology, University of Auckland, Auckland, New Zealand

²Manaaki Manawa Centre for Heart Research, University of Auckland and Pūtahi Manawa Centre of Research Excellence, Auckland, New Zealand

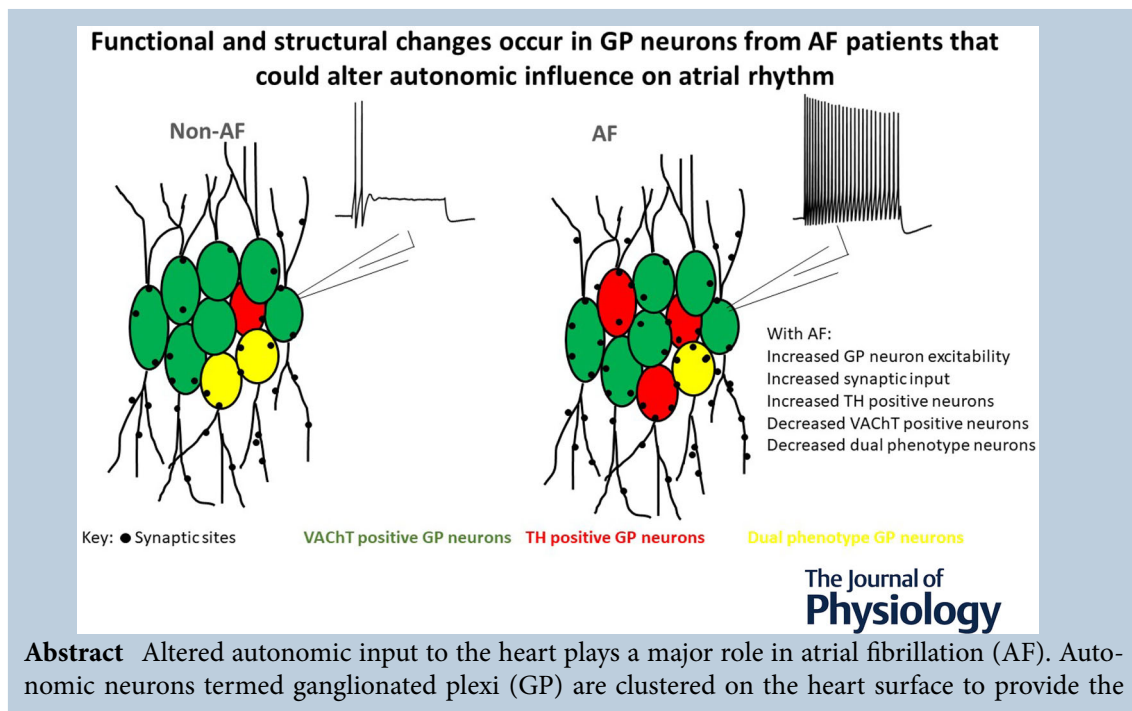
³Auckland Bioengineering Institute, University of Auckland, Auckland, New Zealand

⁴Cardiothoracic Surgical Unit, Auckland City Hospital, Auckland, New Zealand

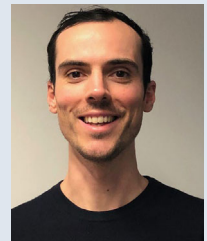
⁵Department of Cardiology, Auckland City Hospital, Auckland, New Zealand

Handling Editors: Harold Schultz & Andrew Holmes

The peer review history is available in the Supporting Information section of this article (<https://doi.org/10.1113/JP286278#support-information-section>).



Jesse Ashton gained his PhD in Bioengineering and Physiology at the University of Auckland. He then performed postdoctoral research in Physiology examining the physiological and structural properties of rodent and human intracardiac neurons. He shifted from a Research Fellow at the University of Auckland to a Senior Data Analyst at PredictHQ. In his new role, he applies his expertise in data analysis and statistics to enhance predictive models for business demand, focusing on insights from local events. His work supports strategic decision-making, demonstrating his commitment to leveraging data for actionable business intelligence.



last point of neural control of cardiac function. To date the properties of GP neurons in humans are unknown. Here we have addressed this knowledge gap in human GP neuron structure and physiology in patients with and without AF. Human right atrial GP neurons embedded in epicardial adipose tissue were excised during open heart surgery performed on both non-AF and AF patients and then characterised physiologically by whole cell patch clamp techniques. Structural analysis was also performed after fixation at both the single cell and at the entire GP levels via three-dimensional confocal imaging. Human GP neurons were found to exhibit unique properties and structural complexity with branched neurite outgrowth. Significant differences in excitability were revealed between AF and non-AF GP neurons as measured by lower current to induce action potential firing, a reduced occurrence of low action potential firing rates, decreased accommodation and increased synaptic density. Visualisation of entire GPs showed almost all neurons are cholinergic with a small proportion of noradrenergic and dual phenotype neurons. Phenotypic distribution differences occurred with AF including decreased cholinergic and dual phenotype neurons, and increased noradrenergic neurons. These data show both functional and structural differences occur between GP neurons from patients with and without AF, highlighting that cellular plasticity occurs in neural input to the heart that could alter autonomic influence on atrial function.

(Received 30 January 2024; accepted after revision 22 March 2024; first published online 1 May 2024)

Corresponding author J. M. Montgomery: Department of Physiology, Faculty of Medical and Health Sciences, 85 Park Rd, Grafton, Auckland, New Zealand. Email: jm.montgomery@auckland.ac.nz

Abstract figure legend Cartoon rendition of properties of human GP neurons from non-AF (left) and AF (right) patients. In AF patients, there are significantly fewer cholinergic neurons, more noradrenergic neurons, and fewer dual-phenotype neurons compared to GP neurons from non-AF patients. Cellular electrophysiological studies show GP neurons also fire action potentials for a longer time duration in AF patients compared to non-AF patients. Together these data show both functional and structural differences occur in GP neurons from non-AF vs. AF patients, highlighting that cellular plasticity occurs in neural input to the heart that could alter autonomic influence on atrial function.

Key points

- The autonomic nervous system plays a critical role in regulating heart rhythm and the initiation of AF; however, the structural and functional properties of human autonomic neurons in the autonomic ganglionated plexi (GP) remain unknown.
- Here we perform the first whole cell patch clamp electrophysiological and large tissue confocal imaging analysis of these neurons from patients with and without AF.
- Our data show human GP neurons are functionally and structurally complex. Measurements of action potential kinetics show higher excitability in GP neurons from AF patients as measured by lower current to induce action potential firing, reduced low firing action potential rates, and decreased action potential accommodation.
- Confocal imaging shows increased synaptic density and noradrenergic phenotypes in patients with AF.
- Both functional and structural differences occur in GP neurons from patients with AF that could alter autonomic influence on atrial rhythm.

Introduction

The intrinsic cardiac nervous system (ICNS) is part of the autonomic nervous system that forms neural circuits in the heart. The ICNS integrates control signals from higher neuronal centres, transmitted via sympathetic and parasympathetic nerves, with sensory feedback from neurons in the heart and thorax to provide local

coordination of heart rate and rhythm (Armour et al., 1997; Ardell & Armour, 2016). The ICNS consists of multiple, interconnected ganglia – termed ganglionated plexi (GP) – that are made up of efferent and sensory afferent neurons, as well as local circuit neurons, which exhibit diverse neurochemical phenotypes (Edwards et al., 1995; Armour et al., 1997; Richardson et al., 2003; Hoover et al., 2009). GPs are embedded in adipose tissue on the

epicardial superficial surface of the myocardium at the roots of the great vessels and at the base of the ventricles, comprising an estimated 14,000–43,000 neurons (Ardell & Armour, 2016; Pauza et al., 2000). GPs in specific anatomic locations have been shown to exert control over distinct regions of the heart. For example, the right atrial GPs (RAGP) anterior to the right superior pulmonary has been shown to mediate vagal control over the sinoatrial node (Rajendran et al., 2019).

Intracellular and whole cell patch clamp recordings have been performed on individual GP neurons in rodents (Edwards et al., 1995; Rimmer & Harper, 2006; McAllen et al., 2011; Ashton et al., 2020) and reveal heterogeneous electrophysiological properties with diverse action potential kinetics, ability to fire bursts of action potentials, rectification properties, afterhyperpolarisation duration and synaptic input. Morphologically, GP neuron architecture differs between mammalian species, with varied relative contributions of unipolar, pseudo-unipolar and multipolar neurons, and large differences in total dendritic area and axon length (Richardson et al., 2003; Edwards et al., 1995; Horackova et al., 1999). Dipolar and pseudodipolar morphologies have been associated with sensory phenotypes, whereas multipolar neurons are thought to have at least one projection to the myocardium and be of efferent nature (Edwards et al., 1995).

Aberrant autonomic nerve activity within the ICNS is known to contribute significantly to the pathogenesis of atrial fibrillation (AF). In both animal models and humans, altered GP output and the remodelling of myocardial innervation have been found to correlate with AF (e.g. Ashton et al., 2020; Lim et al., 2011; Salavatian et al., 2016; Tan et al., 2008; Smith et al., 2023; Ashton et al., 2018). Thus, pathophysiological conditions which modify the physiological properties of GP neurons or the strength of their neurotransmission – i.e. neuronal plasticity – have the potential to profoundly influence susceptibility to AF. Consistent with this, we have recently shown that atrial arrhythmia in the spontaneously hypertensive rat model correlates with increased activity at GP neuron synapses as well as increased synapse density, supporting a role for neural plasticity in arrhythmia substrate (Ashton et al., 2020).

As the ICNS is the last point of neural control of the heart, it is a target for strategies aimed at improving AF treatment (Linz et al., 2014; Armour, 2008; Kron et al., 2010; Buckley et al., 2016). In order to refine these therapies, it is critical that we develop a greater understanding of the physiological properties of ICNS neurons and how these change with AF, particularly in humans where no cellular electrophysiological recordings have been made and hence no knowledge exists of their physiological properties. Here we have performed pioneering cellular electrophysiological recordings in human GP

Table 1. Summary of patient data

	Non-AF	AF
Age (years)	66.16 ± 5.89	69.67 ± 11.32
Sex, female (n (%))	6/25 (24%)	3/12 (25%)
BMI (kg/m ²)	30.06 ± 6.82	25.99 ± 3.98
Hypertensive (n (%))	17/25 (68.00%)	7/12 (58.33%)
Diabetes (n (%))	5/25 (20.00%)	1/12 (8.33%)
Hyperlipidaemia (n (%))	14/25 (56.00%)	5/12 (41.67%)
Beta blockers (n (%))	13/25 (52.00%)	6/12 (50.00%)
Persistent AF (n (%))	0/25 (0%)	10/12 (83.3%)
Paroxysmal AF (n (%))	0/25 (0%)	2/12 (16.7%)

neurons from patients with and without AF and have imaged entire ganglia in both. Our data reveal that distinct structural and functional differences in GP neurons are associated with AF as compared to controls, which suggests ICNS plasticity contributes to the AF substrate in humans and therefore could be a target to decrease excitability in GPs.

Methods

Ethical approval

All procedures were approved by the New Zealand Health and Disability Ethics Committee (18/CEN/99), as well as the Auckland District Health Board Research Review Committee (ADHB number A+8285). After informed consent was obtained in writing from patients undergoing open heart surgery for coronary artery bypass grafting and/or valve repair (Table 1), surgical biopsies of cardiac epicardial adipose tissue from the RAGP were collected. These studies conformed to the standards set by the latest version of the *Declaration of Helsinki*, except for registration in a database. All investigators understand the ethical principles for human experiments under which *The Journal of Physiology* operates.

Collection of surgical biopsies

Adipose tissue was resected as previously described (Hoover et al., 2009) in the region of the right atrial ganglionated plexus (RAGP) located anterior to the right superior pulmonary vein, partially overlapping the Waterston groove and lateral right atrial free wall. Held from the lateral epicardial edge, adipose tissue samples up to 10 mm³ were removed by careful separation from the atrial myocardium using sharp dissection without damaging the underlying muscle. Samples were then transferred immediately to the laboratory on ice in carbogen bubbled *N*-methyl *D*-glucamine (NMDG)-based extracellular solution (composition in mmol/l: 93 NMDG, 2.5 KCl,

1.2 NaH₂PO₄, 30 NaHCO₃, 20 HEPES, 25 glucose, 5 L-ascorbic acid, 2 thiourea, 3 sodium pyruvate, 10 MgSO₄, 0.5 CaCl₂, pH 7.35–7.4; Ting et al., 2014).

Adipose slice preparation

Epicardial adipose samples were cut into 0.5–1.0 mm-thick slices either parallel or orthogonal to the visceral pericardial layer with a tissue slicer (model 51425, Stoelting, Wood Dale, IL, USA) and placed in fresh NMDG-based extracellular solution, cooled to 4°C and continuously gassed with carbogen (5% CO₂, 95% O₂). Slice preparations were gently held by nylon mesh between two stainless steel washers and then incubated in carbogenated NMDG-based extracellular solution with collagenase B (0.75 mg/ml, Sigma-Aldrich, Auckland, New Zealand) and trypsin (5 mg/ml, T4799, Sigma-Aldrich) at 37°C for 1 h to soften the connective tissue sufficiently to enable access to GP neurons while maintaining the structural integrity of the ganglia. Slice preparations were then stored in carbogenated extracellular solution (composition in mmol/l: 97 NaCl, 2.5 KCl, 1.2 NaH₂PO₄, 30 NaHCO₃, 20 HEPES, 25 glucose, 5 L-ascorbic acid, 2 thiourea, 3 sodium pyruvate, 2 MgSO₄, 2 CaCl₂, pH 7.35–7.4) at room temperature (22°C).

Whole-cell patch clamp recordings

Adipose slice preparations were mounted in the recording chamber on an upright microscope (Axioskop, Zeiss Microscopy, Jena, Germany) and perfused via gravity feed with carbogenated artificial cerebrospinal fluid at 35°C. Using infra-red differential interference contrast (IR-DIC) optics and a ×40 objective, GP neurons were found in ganglia embedded within adipose and connective tissue adjacent to nerve fibre tracts. Glass microelectrodes (resistance 6–8 MΩ) were filled with internal solution (composition in mmol/l: 120 potassium gluconate, 40 HEPES, 5 MgCl₂, 2 NaATP, 0.3 NaGTP, pH 7.2 with KOH). These microelectrodes were used to gently separate the satellite glial cell sheath from the neuronal membrane as previously described (Ashton et al., 2020) before obtaining whole-cell patch clamp recordings from the visualised neurons. Fluor 568 hydrazide (Alexa, Thermo Fisher Scientific, Waltham, MA, USA; 50 μmol/l) was included in the internal solution to enable identification of neurons in subsequent imaging (Wang et al., 2013). All analyses of whole cell patch clamp data were performed in Clampex (pCLAMP 10.6, Molecular Devices, San Jose, CA, USA) and using custom scripts written in MATLAB (The MathWorks, Inc., Natick, MA, USA) as described in our previous work (Ashton et al., 2020;

Lee et al., 2020; Park et al., 2020; Lee et al., 2022; Vyas et al., 2020). A junction potential of +10 mV was calculated, and membrane potential measurements were adjusted accordingly. Passive membrane properties were determined by averaging measurements from 10 × 10 mV voltage steps taken in voltage clamp mode at a holding potential of –70 mV. To calculate the cell membrane time constant τ , we fitted an exponential function of the form $I(t) = B + me^{-t/\tau}$ to the current decay transient, where B and m are constants which represent the steady state current during the voltage step and the peak transient current relative to this, respectively. Action potential frequency was counted within 1000 ms current steps from 200 to 1000 pA. The interspike interval (ISI) between the first pair and the last pair of action potentials within a current step (1000 pA, 1000 ms) was used to measure accommodation of action potential firing. Accommodating neurons were defined as those with an ISI ≥ 1.5 and non-accommodating neurons as those with an ISI ≤ 1.5 (Adke et al., 2021).

Confocal microscopy of dye-filled neurons

Images of dye-filled GP neurons were captured using a FluoView1000 laser scanning confocal microscope (Olympus, Tokyo, Japan) fitted with 0.8 NA/×20 water immersion and 1.35 NA/×63 silicone oil immersion objectives (Olympus) and controlled with the FluoView 4.2 software suite (Olympus). For ×60 images, individual voxels were 0.1 × 0.1 × 0.5 μm (x, y, z) in size with the pinhole set to 1 Airy unit. For ×20 images, the pinhole diameter was adjusted to maximise information capture for each sample and so, although voxels consistently measured 0.31 × 0.31 μm in the x and y directions, voxel size in the z axis was variable. The image field was set so that the neuronal soma and all peri-somatic dendrites were captured in ×60 images and the entire neuron, including all detectable processes, in ×20 images. Offset and photo-multiplier tube gain were adjusted for each image to optimise data collection.

Unless stated otherwise, data processing and analysis were carried out using ImageJ (NIH, Bethesda, MD, USA). Imaging the distribution of the dye injected into the neuronal soma during whole cell patch-clamp recording enabled the creation of masks for individual GP neurons. These images were denoised using the despeckle function and then smoothed with a Gaussian filter ($\alpha = 1$). Background signal was removed by subtracting intensity from the entire image equal to the mean grey area for a representative background region. Segmentation was achieved using the random forest classifier in the open-source software platform ITK-SNAP (<http://www.itksnap.org>), and morphology was measured from the resulting cell mask.

Tissue clearing, immunohistochemistry, and confocal imaging of adipose slices

Fixed epicardial adipose samples were sliced at 1 mm thickness orthogonal to the visceral pericardial layer, washed in phosphate-buffered saline (PBS) and embedded in 2% agarose before tissue clearing, as described in our recent work (Sands et al., 2022). Sequential hydrophilic (CUBIC R1) and hydrophobic processes were used to clear neural tissue and fat in epicardial slices. Samples were immersed in 50/50 ratio of CUBIC R1/H₂O for 5 days, refreshed at 48 h intervals, followed by dehydration in a graded series of methanol (25%, 50%, 75%, 95%) and maintenance in 100% methyl salicylate for 5 days. Dehydration gradient incubations were reversed to enable immunostaining, and slices were stored in PBS + sodium azide (0.025%). Immunohistochemistry was performed as described below followed by hydrophilic clearing and refractive index matching by transferring slices to 100% Ce3D via gradient steps at 50% and 80% (Li et al., 2017). Slices were suspended in 100% Ce3D for a minimum of 8 days before confocal imaging.

For immunostaining, slice preparations were incubated with primary antibody dissolved in blocking solution (5% normal donkey serum, 0.5% Triton X-100 in 1 × PBS) for 5 days at 37°C. Primary antibodies used in this study were: rabbit anti-synapsin1, 1:500, cat. no. S193, Sigma-Aldrich; sheep anti-tyrosine hydroxylase (TH), 1:250, cat. no. AB1542, Sigma-Aldrich; guinea pig anti-Vesicular acetylcholine transporter (VAcHT), 1:500, cat. no. 139105 Synaptic Systems, Göttingen, Germany. Slices were then washed in PBS + 0.025% sodium azide then incubated in AlexaFluor conjugated secondary antibodies for 5 days at room temperature (1:200, anti-rabbit Alexa Fluor 568 or 647, cat. no. 711-605-152, Jackson ImmunoResearch Laboratories, West Grove, PA, USA).

Images were acquired using a custom stage-scanning line confocal microscope with a ×25 objective lens (Olympus XLSLPLN25XGMP, 1.0 NA, 8 mm WD, Refractive Index 1.41–1.52 (Sands et al., 2022)). Initial low-resolution *z*-stacks (1 × 1 × 50 μm voxels) were acquired of entire epicardial slices to determine ganglia locations enabling the inclusion of entire ganglia in the visual field. High-resolution *z*-stacks (1 × 1 × 1 μm voxels) were then acquired from all locations where ganglia were visually identified. Images were deconvolved using a measured point spread function (PSF) with 40 iterations of the Richardson–Lucy algorithm. Ganglia from adipose slices immunolabelled with synapsin1 were reimaged at higher magnification (0.2 × 0.2 × 0.5 μm voxels) on a point confocal microscope (Olympus FV1000) with a ×60 silicone oil immersion objective (NA 1.35). Amplifier gain and offset were adjusted to accommodate the entire dynamic range of the signal within each ganglion stack.

Image analysis was performed with FIJI, an enhanced version of ImageJ software, as described in our previous studies (e.g. Ashton et al., 2020; Lee et al., 2022; Vyas et al., 2020). Analysis was performed blinded to AF status. *Z*-series images were merged into maximal projection images for manual counts of TH and VAcHT-positive neurons. Regions of interest (ROI) were drawn around every neuron soma. Cells with double nuclei or severe distortion were excluded from the selection. From a complete ROI set for each ganglion, ROIs with colocalised labelling for a second marker (TH) were duplicated in a second ROI set. The percentage of TH-positive ROIs that colocalised with VAcHT-positive ROIs was calculated according to the number of TH positive ROIs divided by the number of VAcHT positive ROIs, multiplied by 100.

VAcHT immunofluorescence was used to define the image mask of the cholinergic neuronal soma and proximal regions of adjoining fibres. Background subtraction and segmentation of synaptic puncta were achieved via a Gaussian filtered ($\alpha = 5$ pixels) duplicate subtracted from each image to remove the background signal. The signal representing synaptic puncta was then segmented using an iterative thresholding technique (volume $\geq 1 \mu\text{m}^3$, minimum intensity threshold, mean image intensity + 2 × standard deviation). Total synapse count per ganglion was achieved by analysing high-resolution *z*-stacks acquired from the stage-scanning line confocal microscope enabling whole ganglion masks to be used for segmentation. Synapsin1 puncta density was normalised to area as number of puncta per 10,000 μm³ as in our previous work (Lee et al., 2022). For each data set, the image analysis criteria including intensity threshold and detection voxel size range were kept consistent.

Statistical analysis

Unless otherwise stated, data are presented as means ± standard deviation (SD). A subset of data are presented as median and 95% confidence intervals (CIs) (median, lower interval, upper interval). Statistical analyses were conducted using Graphpad Prism 8.2.1 (GraphPad Software, San Diego, USA), with a *P*-value ≤ 0.05 considered significant. The Shapiro–Wilk normality test was performed to assess normality and homogeneity of variances in the data. Statistical significance was determined by Student's *t* test for comparison between two groups with normally distributed data. For non-normally distributed data, a Mann–Whitney test was used to compare ranks. The Kolmogorov–Smirnov test was applied to compare soma size distributions between two groups. Significance of results are marked with ns (non-significant), $P > 0.05$, * $P \leq 0.05$, ** $P \leq 0.01$, *** $P < 0.001$ and **** $P < 0.0001$.

Results

Intracellular dye filling reveals complex morphology of human GP neurons

We first sought to examine the morphology of human GP neurons via confocal imaging of GP neurons that were able to be successfully dye-filled during whole-cell patch clamp recordings (Fig. 1A–D; $n = 8$ neurons from $n = 6$ patients). In comparison to similar cell fills performed in rodent GP neurons (Ashton et al., 2020), the significant increase in neuronal complexity and the multipolar nature of human GP neuron morphology was immediately evident, as shown by the high degree of neurite branching and outgrowth (Fig. 1A and B). Human GP neurons were observed to have multiple primary neurites extending from the neuronal soma, ranging from 4 to 11 (mean = 7.4 ± 1.17). These were presumed to be dendrites based on their extensions from the soma remaining within a field close to the neuron. In addition, a high density of

synaptic sites formed onto these processes, as evidenced by the high number of synapsin1 puncta (Fig. 1C). Some GP neurons had many primary dendrites with few or no branches leading to lower total dendrite length. Dendrites were also frequently observed to form a ‘halo’ that enveloped the neuronal soma and were highly dense in synaptic contacts (Fig. 1C and D). One primary neurite in each neuron was often observed to extend hundreds of micrometres beyond the field of view from the cell body and branch significantly, possibly representing axons extending towards other ganglia. Growth cones were also evident at the end of neurites (Fig. 1B). On mean, total neurite length was $499.04 \pm 261.37 \mu\text{m}$, but this varied widely from neuron to neuron, ranging from 139.27 to $2319.86 \mu\text{m}$. The total number of branches also varied from neuron to neuron, ranging from 1 to 13 (mean 5.71 ± 1.91 branches). Total neurite area of human GP neurons ranged from 3396.18 to $6254.90 \mu\text{m}^2$ (mean area was $4948.09 \pm 588.45 \mu\text{m}^2$). Together these data show

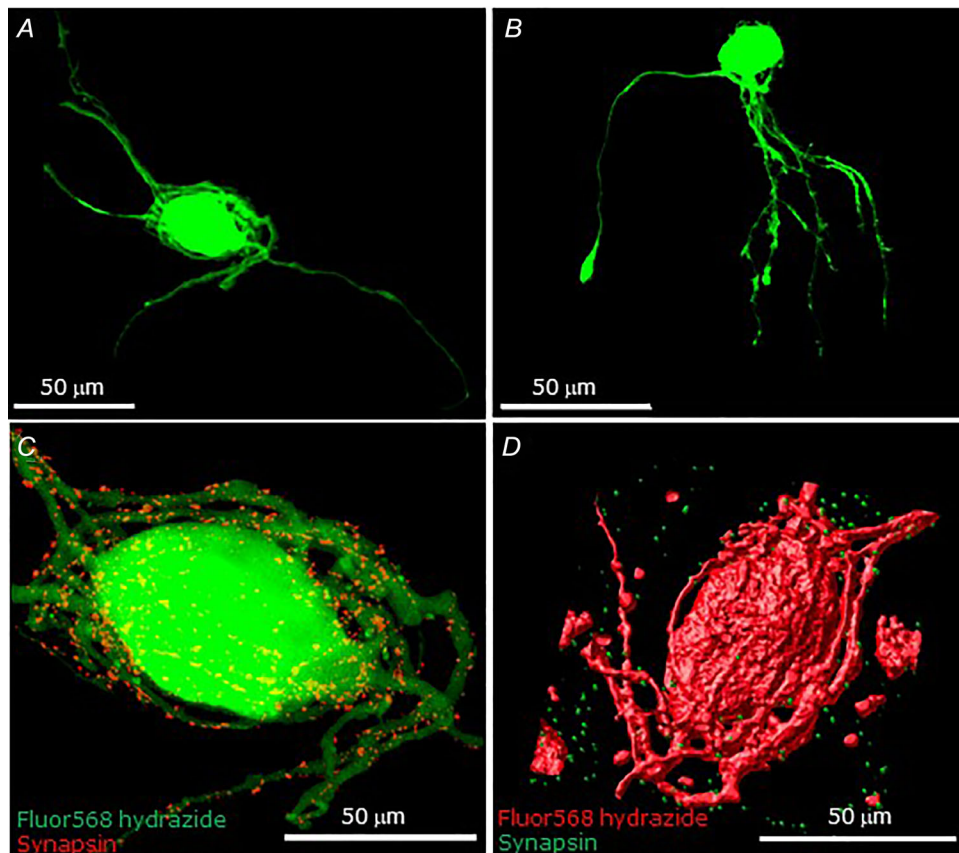


Figure 1. Human GP neuron morphology

GP neurons were filled with Fluor 568 hydrazide during whole cell patch clamp recordings and imaged by confocal microscopy. A and B, example successful fills of GP neurons showing complex and varied morphology. Neurites are observed to branch and extend significantly from the cell body. Scale bar $50 \mu\text{m}$. C, zoomed image of the soma region of the GP neuron depicted in A. Note the wrapping of the neurites around the soma. Synapsin immunostaining is shown in red. Scale bar $50 \mu\text{m}$. D, 3D isosurface image of the filled GP neuron in A (red) with synapsin puncta (green). Scale bar $50 \mu\text{m}$.

that human GP neuronal structure is highly complex and indicate extensive networks among neurons both within and between GP.

Human GP neuron electrophysiological properties revealed by whole cell patch clamp

Whole cell patch clamp recordings were performed on RAGP neurons from patients with and without AF (Table 1; Figs 2–4). The RAGPs are known to contribute to neural control of the sinus node and stimulation of the RAGPs has also been shown to induce AF in large animal models (Hanna et al., 2021; Cardinal et al., 2009; Gibbons et al., 2012). Within the adipose slices containing GPs, ganglia were typically found along nerve fibre tracts or at branch points embedded within adipose and connective tissue close to the cut surface of RAGP slice preparations. Figure 2A shows a photomicrograph of a typical *in situ* ganglion taken using IR-DIC microscopy. GP neurons were readily identified from spherical adipocytes by their densely packed large ovoid cell bodies with primary neuronal processes extending into as well as away from the ganglia.

Whole cell patch clamp recordings were performed in both current clamp and voltage clamp mode to enable measurements of passive membrane properties, excitability, action potential kinetics and firing patterns in human GP neurons (Figs 2–4). Membrane tests to determine passive and active membrane properties (see Methods) were performed on 25 GP neurons from 18 patients. No significant difference was observed in resting membrane potential in GP neurons from patients with AF compared to those without AF. Mean RMP was -62.97 ± 9.19 mV in non-AF GP neurons, vs. -62.55 ± 8.68 mV in GP neurons from AF patients ($P = 0.917$; Fig. 2B), indicating good neuronal health in both groups. No significant differences were observed in membrane capacitance between GP neurons from non-AF vs. AF patients (187.1 ± 17.74 pF vs. 159.92 ± 13.92 pF, non-AF vs. AF, $P = 0.241$), or between either series resistance (non-AF 12.61 ± 4.58 M Ω vs. AF 15.41 ± 4.11 M Ω ; $P = 0.164$) or membrane resistance (non-AF 243.31 ± 38.52 M Ω vs. AF 320.04 ± 41.52 M Ω , $P = 0.194$; Fig. 2C–E).

Human GP action potential kinetics were determined in current clamp mode and were similar in GP neurons from AF and non-AF patients (Fig. 3A–F). There was no significant difference in mean action potential amplitude (non-AF 58.3 ± 10.6 mV vs. AF 58.2 ± 12.6 mV; $P = 0.988$), membrane threshold potential for single evoked action potentials (non-AF -32.9 ± 6.3 mV vs. AF -33.4 ± 6.0 mV; $P = 0.862$) or action potential half-width (non-AF 1.10 ± 0.47 ms vs. AF 1.36 ± 0.57 ms; $P = 0.323$) in GP neurons from AF vs. non-AF patients (Fig. 3B–D).

Single evoked action potentials with both short and long after-hyperpolarisations were observed and there were no significant differences in after-hyperpolarisation decay time (non-AF 50.8 ± 36.4 ms vs. AF 64.9 ± 49.2 ms; $P = 0.541$) or magnitude (non-AF -12.0 ± 6.1 mV vs.

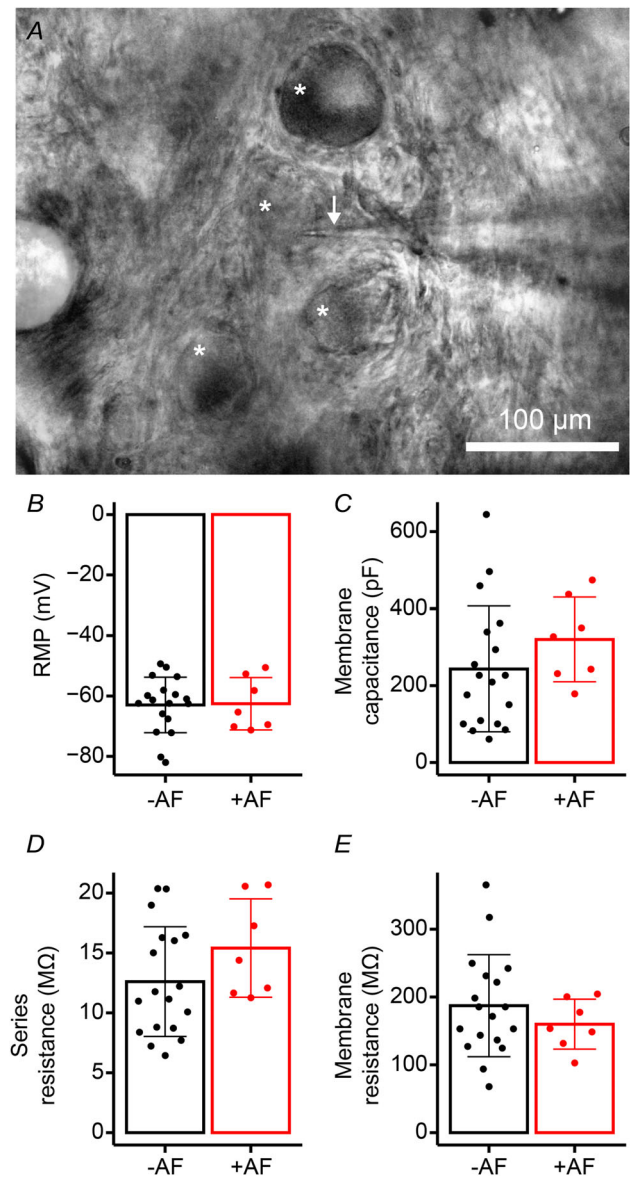


Figure 2. Passive membrane properties are similar in human GP neurons from non-AF and AF patients

A, photomicrograph of GP neurons and adipocytes in a typical *in situ* ganglion taken under IR-DIC microscopy. GP neurons (white asterisks) are readily identified by their densely packed large, ovoid cell bodies. The white arrow indicates the glass patch electrode. B–E, passive membrane properties were measured from $n = 18$ non-AF GP neurons and $n = 7$ AF GP neurons, taken from $n = 13$ non-AF and $n = 5$ AF patients. No significant difference was detected in RMP (B), membrane capacitance (C), series resistance (D), or membrane resistance (E) between GP neurons from non-AF (black) and AF (red) patients (Student's *t* test).

AF -13.5 ± 6.5 mV; $P = 0.605$) between non-AF and AF patients (Fig. 3E and F). There was also no difference in the steady-state current response to hyperpolarising voltage steps from -50 mV to -125 mV in AF compared to non-AF patients ($P = 0.540$ for the effect of AF).

Next we measured action potential firing frequency in response to prolonged (1000 ms) steps of increasing current injection amplitude in both AF and non-AF GP neurons (Fig. 4A–E). Action potential firing was examined in a total of 24 GP neurons ($n = 16$ non-AF and

$n = 8$ AF, from $n = 11$ non-AF patients and $n = 6$ AF patients). In GP neurons from non-AF tissue, failure to fire action potentials occurred at a total frequency of 37.5% (throughout all current steps), compared with 12.5% in GP neurons from AF tissue. At the initial current step of 200 pA, action potential failure occurred at a frequency of 31.35% in GP neurons from non-AF tissue, compared with 0% in GP neurons from AF tissue. Examining the relative frequencies of action potential number at each current step (Fig. 4A and B) showed GP neurons from non-AF patients exhibited a broader range of AP firing frequency, and notably showed a higher frequency of low firing neurons (range 0 to 5 action potentials/1000 ms) compared with GP neurons from AF patients (non-AF: percentage GP neurons with low action potential frequency 29.17%; AF: percentage GP neurons with low action potential frequency 12.50%). This was balanced by an increased frequency of medium-rate spiking neurons (range 10–15 action potentials/1000 ms) in GP neurons from AF patients (non-AF: percentage GP neurons with medium action potential frequency 14.58%; AF: percentage GP neurons with medium action potential frequency 33.33%) as seen by the rightward shift in the frequency histogram (Fig. 4B). GP neurons from AF and non-AF patients showed a similar frequency of high spiking neurons (15 or more action potentials/1000 ms; non-AF: 44.75% and AF: 39.58%; Fig. 4B).

These differences in action potential firing raise the possibility that GP neurons from AF patients require less current to induce action potential firing. This is measured as action potential rheobase, defined as the amount of current required to induce action potential firing. Rheobase was measured between GP neurons from AF ($n = 6$) vs. non-AF patients ($n = 12$), and was significantly lower in GP neurons from AF patients compared with non-AF patients (non-AF: 0.80 ± 0.56 pA/pF vs. AF: 0.35 ± 0.15 pA/pF; $P = 0.027$; Fig. 4C).

GP neurons from AF and non-AF patients also responded to prolonged current injection with accommodating and non-accommodating AP firing patterns (Fig. 4D). Quantification of accommodation in action potential firing, as measured by the relative change in inter-spike interval (ISI) between the first pair and last pair of action potentials (Adke et al., 2021), was performed in $n = 16$ GP neurons from $n = 11$ non-AF patients and $n = 8$ GP neurons from $n = 6$ AF patients. GP neurons from non-AF tissue were almost all accommodating neurons that slowed their firing frequency with time (93.75%). In GP neurons from AF tissue, a lower frequency of accommodating neurons was observed (62.5%) and therefore a higher frequency of fast-spiking neurons that did not accommodate (37.5% in AF GP neurons vs. 6.25% in non-AF GP neurons; Fig. 4E).

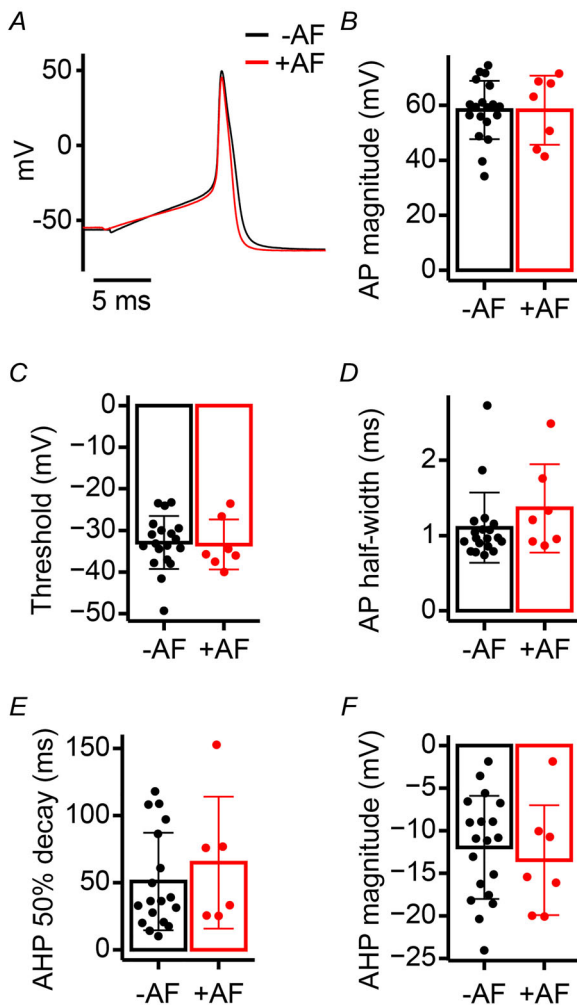


Figure 3. Action potential kinetics of human GP neurons

A, example single action potential (AP) traces from whole cell patch clamp recordings from GP neurons from non-AF (black) and AF (red) patients. Active membrane properties were measured from $n = 18$ non-AF GP neurons and $n = 7$ AF GP neurons, taken from $n = 13$ non-AF and $n = 5$ AF patients. B–D, no significant differences were observed in action potential mean magnitude/amplitude (B), threshold potential (C), or half-width (D) between GP neurons from non-AF and AF patients (Student's *t* test). E and F, there was also no significant difference in after-hyperpolarisation (AHP) decay (E) or AHP magnitude (F) between non-AF and AF GP neurons (Student's *t* test).

Structural plasticity at human GP neuron synapses

To examine synaptic input onto human GP neurons, which may contribute to changes in GP neuron excitability, we measured synapsin1 expression in the GP neurons of patients with and without AF (Fig. 5A–G; imaging performed on 19 ganglia from $n = 5$ non-AF and $n = 5$ AF patients). Synapsin1 is a protein that condenses synaptic vesicles to the synaptic vesicle cluster associated with the active zone in presynaptic boutons, and consequently synapsin1 shows localisation of presynaptic sites (Ashton et al., 2020; Lee et al., 2022). Synapsin1 puncta were observed to be densely

packed on both the somas and the dendritic trees of GP neurons (Fig. 1 and Fig. 5A–D), indicating synaptic input throughout the neuron in a pattern similar to complex neurons of the central nervous system (Lee et al., 2020; Park et al., 2020; Vyas et al., 2020; Lee et al., 2022). Quantification of total synapsin1 puncta density in non-AF human GPs showed a mean of 311.31 ± 27.62 synapsin1 puncta/ganglion (ranging from 39 to 484; $n = 9$ ganglia from $n = 5$ non-AF patients). Interestingly, total synapsin1 puncta density was significantly higher in human GPs from patients with AF (mean 461.4 ± 26.42 synapsin1 puncta/ganglion, range 128 to 939; $P = 0.05$; $n = 10$ ganglia from $n = 5$ AF patients). This difference

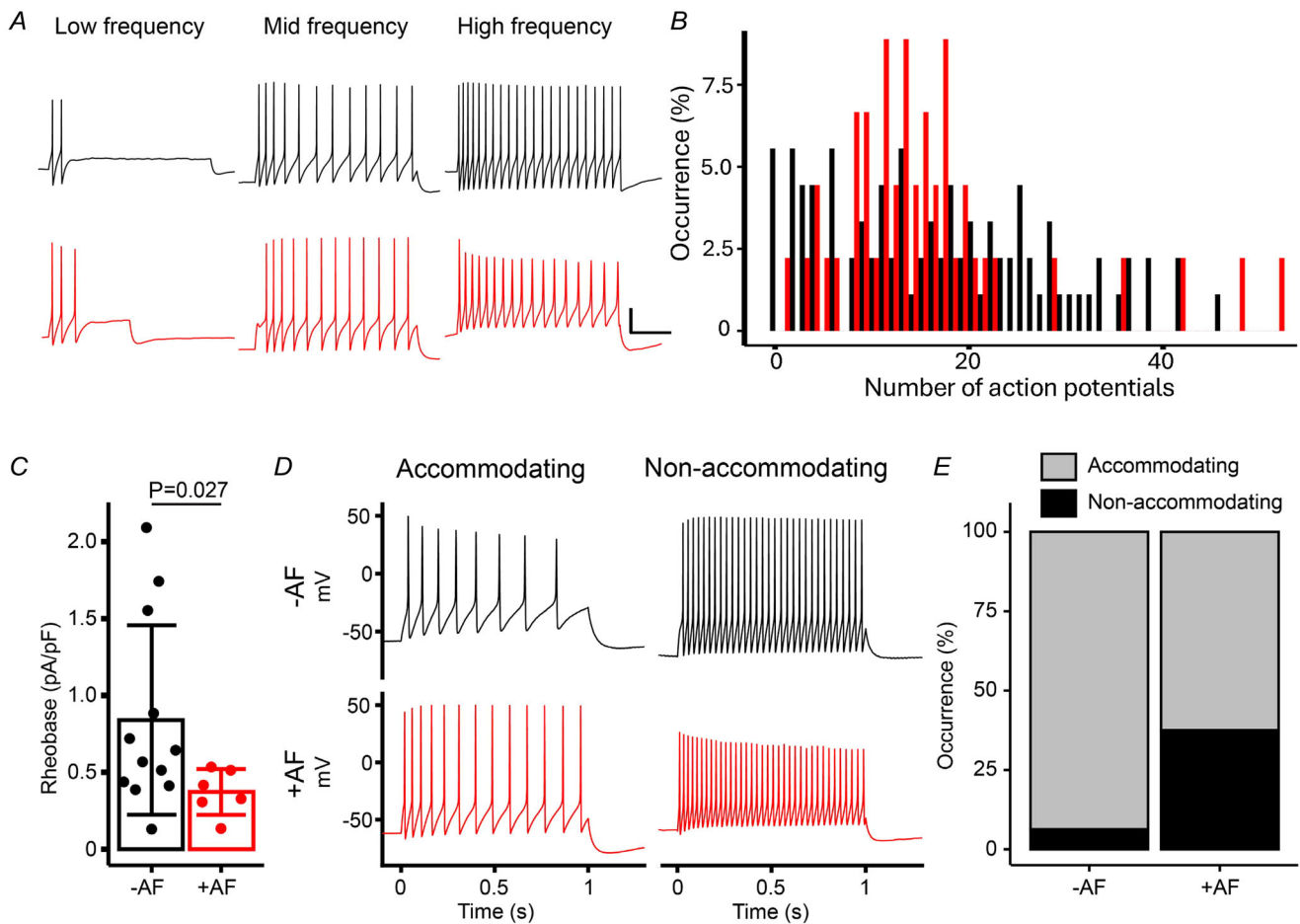


Figure 4. Action potential threshold and firing patterns identify differences in excitability in GP neurons from AF and non-AF patients

A, example traces of low, mid and high action potential firing frequencies in response to prolonged current steps in GP neurons from non-AF (black, top) and AF (red, bottom) patients. B, frequency histogram of action potential firing frequencies measured from $n = 16$ non-AF GP neurons and $n = 8$ AF GP neurons (from 11 and 6 non-AF and AF patients, respectively). GP neurons from AF patients (red) have a frequency distribution that is significantly shifted towards higher firing frequencies compared to control ($P = 0.029$, Wilcoxon rank sum test). C, rheobase was measured in a total of 18 GP neurons from 18 patients ($n = 12$ non-AF and $n = 6$ AF). Rheobase was significantly lower in GP neurons from AF vs. non-AF patients (Student's t test). D, example traces of accommodating and non-accommodating action potential firing in GP neurons from non-AF (black) and AF (red) patients. E, quantification of the frequency of accommodating (grey) and non-accommodating (black) action potential firing patterns in GP neurons (non-AF: $n = 16$ neurons from 11 patients and AF: $n = 8$ neurons from 6 patients). Scales = 25 mV/250 ms.

was not due to AF-related changes in GP neuron density, as no significant difference was measured in non-AF vs. AF patients (non-AF: 5.23×10^{-6} (3.50×10^{-6} , 6.37×10^{-6}) cells/ μm^3 ; AF: 5.21×10^{-6} (3.19×10^{-6} , 6.83×10^{-6}) cells/ μm^3 ; median (95% CI); $P = 0.99$; Fig. 5E). When calculated as density per unit area, synapsin1 puncta density per 10,000 μm^3 was higher in GPs from AF vs. non-AF patients (non-AF: 51.50 ± 9.90 , vs. AF: 136.97 ± 26.11 ; $P = 0.007$; Fig. 5F). The synapsin1 puncta area was also altered in GPs from AF patients. Specifically, the area of GP neuron cell soma associated synapsin1 puncta was significantly shifted rightward between patients with and without AF ($P = 0.0003$) indicating greater synapsin puncta size in patients with AF (Fig. 5G). The volume of individual synapsin1 puncta surrounding cell soma was also measured in samples from AF and non-AF patients and showed that synapsin volume was higher in AF patients than non-AF ($P = 0.0006$; non-AF 1.543 (1.457, 1.585) μm^3 ; AF 1.650 (1.585, 1.693) μm^3 , median (95% CI)).

Extended volume imaging of human GPs and neuronal phenotypes

We applied our custom stage-scanning line confocal microscope (Sands et al., 2022) to reconstruct the 3D arrangement of GPs in optically cleared human adipose epicardial samples (Fig. 6A), enabling the examination of the overall structure of human GPs and their specific phenotypic characterisation (Fig. 6B–D). Low magnification ‘scout’ images that can visualise up to $30 \text{ mm} \times 30 \text{ mm} \times \sim 2 \text{ mm}$ of tissue show GPs dispersed throughout the epicardial adipose tissue (Fig. 6B). Entire GPs and extensive nerve fibres were able to be visualised, both in cross section and in 3D (Fig. 6B–D). Larger diameter nerve fibres, either VAcHT (green) or TH (red) positive, were visible feeding into and out of each ganglion and coursing through the entire epicardial tissue sample (Fig. 6B–D). High-resolution image volumes of individual GPs (Fig. 6C and D) show both VAcHT (green) and TH (red) positive GP neurons tightly packed within

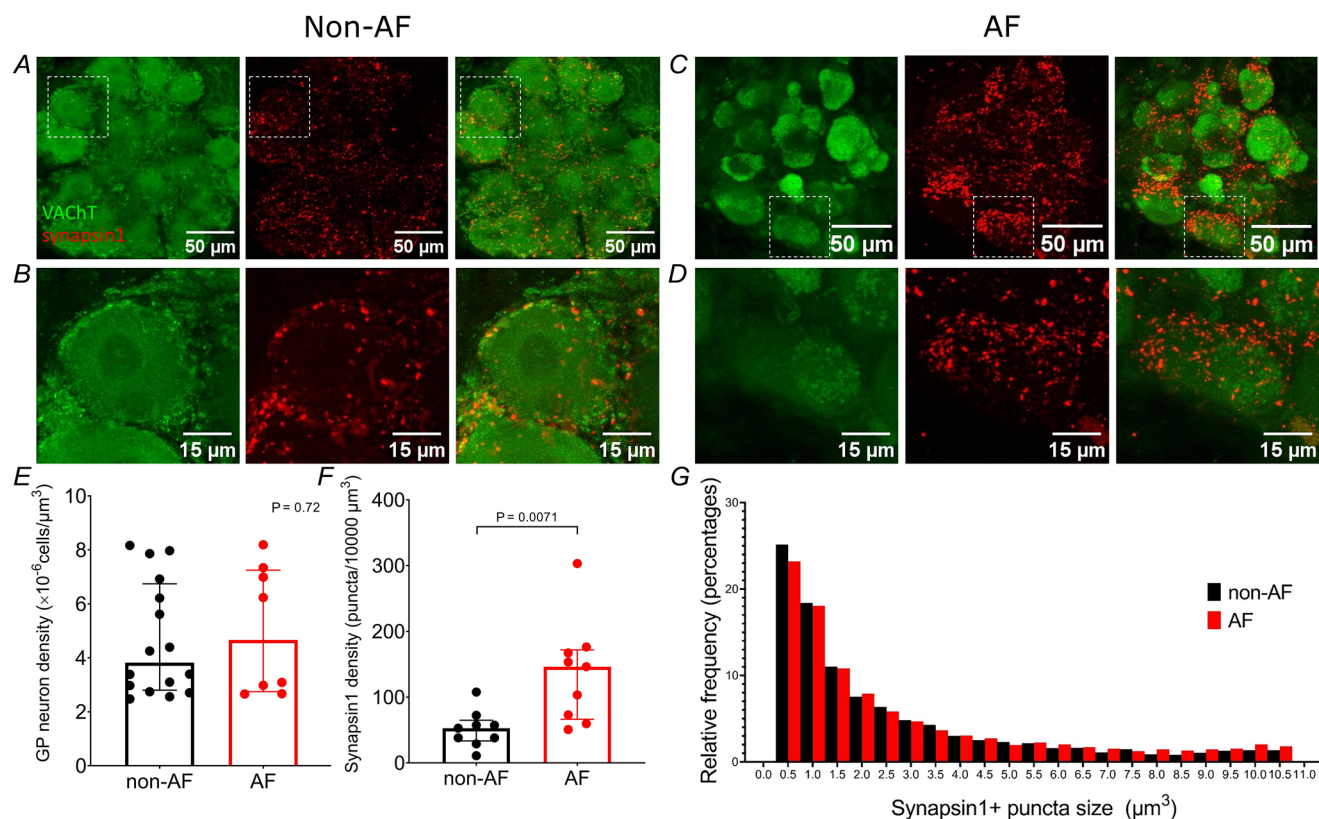


Figure 5. Synapsin immunostaining on human GP neurons shows increased synaptic input with AF
 A–D, example $\times 20$ (top row) and $\times 60$ (bottom row) confocal images of synapsin1 puncta (red) densely packed on the somas and neurites of VAcHT positive GP neurons (green) in non-AF (A and B) and AF (C and D) tissue. E–H, quantification of synapsin1 puncta from $n = 9$ non-AF and $n = 10$ AF ganglia (from $n = 5$ non-AF and $n = 5$ AF patients). E, no significant difference was evident in neuron density between GPs from non-AF and AF patients (Student's *t* test). F, synapsin density per 10,000 μm^3 was significantly higher in GPs from AF vs. non-AF patients (Student's *t* test). G, synapsin puncta area showed a significant right shifted distribution in GPs from AF patients (Kolmogorov–Smirnov test).

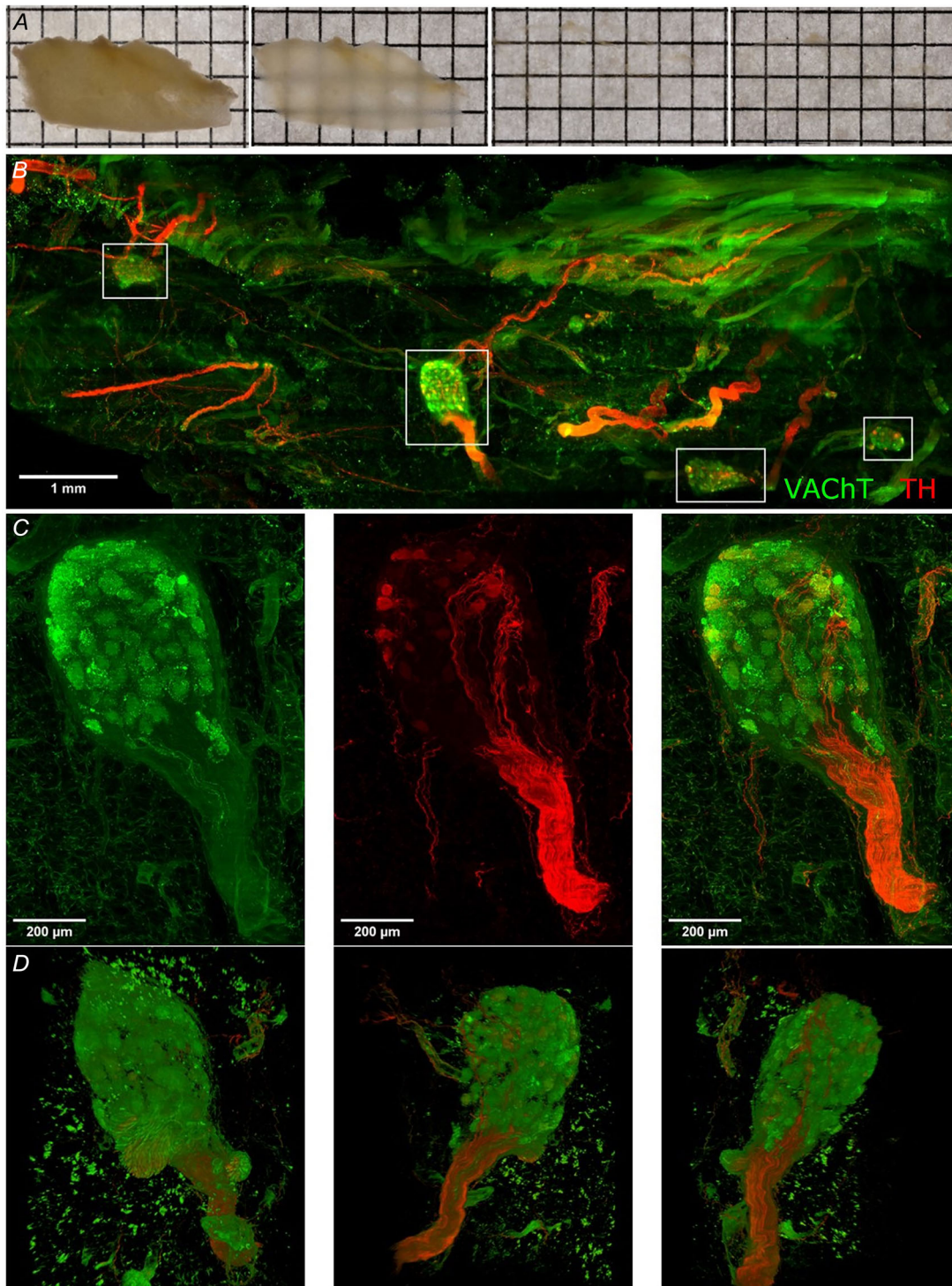


Figure 6. Extended volume imaging of GPs within cleared human adipose samples

A, example images of epicardial adipose tissue progression through the clearing process. Far left: uncleared epicardial adipose tissue in PBS. Middle: after CUBIC-R1 (left) and methyl salicylate (right). Far right: cleared epicardial adipose tissue with refractive index matching in Ce3D. B, example maximal intensity projection scout image showing 10 mm across an epicardial adipose sample. Four GPs are visible dispersed amongst the adipose tissue (boxed) as well as extensive nerve fibres, immunostained for VACHT (green) and TH (red; $0.933 \mu\text{m}$ pixel resolution). C, a maximal intensity projection image ($200 \mu\text{m}$ at $0.933 \mu\text{m}$ spacing) of the central boxed GP, showing VACHT positive cell bodies (green) and TH positive nerve fibres (red). The full image is $880 \times 1276 \times 889$ pixels and has been deconvolved. D, 3D views of the same ganglion in C, visualised with ImageJ 3D viewer with $2\times$ downsampling.

each ganglion, with each containing a range of 11–205 neurons.

We performed phenotypic characterisation of human GP neurons to quantify the relative frequencies of cholinergic and noradrenergic neurons. VACHT immunostaining labelled the vast majority of GP neuronal cell bodies (Fig. 7; $n = 24$ ganglia from $n = 13$ patients). Specifically, $98.57 \pm 0.79\%$ of GP neurons were VACHT-positive in non-AF patients. Interestingly this was significantly higher than in ganglia from AF patients, where $88.52 \pm 3.98\%$ were positive for VACHT ($P = 0.001$; Fig. 7A–F). A small minority of GP neurons showed immunolabelling for TH (Fig. 7B and E): TH positive neurons were observed in 7/8 (87.5%) ganglia from AF patients, compared with only 2/16 (12.5%) ganglia in non-AF patients (Fig. 7G). There was a significant difference in the relative number of TH-positive neurons in AF and non-AF ganglia. In non-AF patient tissue, only $1.09 \pm 0.75\%$ of neurons were TH-positive, compared with $10.42 \pm 3.96\%$ being TH-positive in tissue from AF patients ($P = 0.003$; Fig. 7G).

We observed that a subset of VACHT-positive GP neuronal cell bodies also immunolabelled for TH, suggestive of a dual cholinergic and noradrenergic phenotype as described previously in rodent and human tissue (Fig. 7C and F; Ashton et al., 2020; Clyburn et al., 2022; Clyburn et al., 2023; Ernsberger et al., 1999; Lindh & Hökfelt, 1990; Singh et al., 1999; Weihe et al., 2005). The relative frequencies of dual phenotype GP neurons were significantly different between non-AF vs. AF tissue, with dual phenotype neurons more frequent in non-AF ($28.34 \pm 7.27\%$) than in AF ($2.89 \pm 1.44\%$; $P = 0.023$; Fig. 7G) ganglia.

Discussion

Here we have described the first integrated electrophysiological and imaging examination of human GP neurons from patients with and without AF. Applying our expertise from electrophysiological analysis of human neurons in the central nervous system (Lee et al., 2020; Park et al., 2020) as well as rodent ICNS neurons (Ashton et al., 2020), we were able to develop techniques that enabled access of whole cell patch clamp glass microelectrodes to human GP neurons within epicardial fat pads to examine their cellular physiology and structure. A combination of hydrophilic and hydrophobic clearing techniques then enabled extended volume tissue imaging of entire human GPs. Together this has facilitated a major shift in the ability to examine both the functional and the structural properties of human GP neurons and has identified evidence of remodelling in their properties occurring with AF. The challenges faced with this type of human tissue work are significant, including (1) limited patient consent for the inclusion of additional surgical dissection during complex heart surgery, (2) significantly lower occurrence of AF patients compared to non-AF, and (3) the technical difficulties of locating and accessing GP neurons due to the glial cells ensheathing the soma as well as the surrounding fibrous layer of connective tissue, and the adipose cells significantly limiting visibility. The information gained, however, and the future work this will enable in human tissue over animal models, is critical for our understanding of neural control of heart function and its potential role in arrhythmias that occur in the human heart.

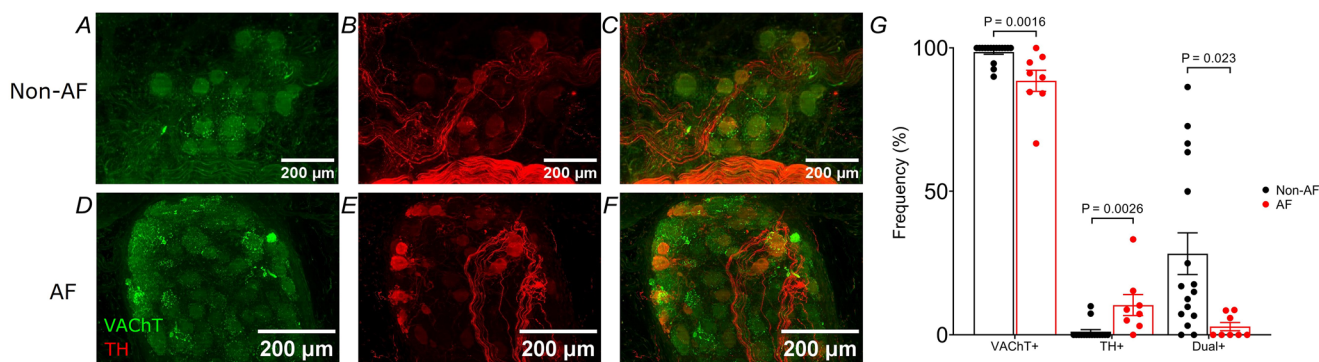


Figure 7. Phenotypic characterisation and quantification of human GP neurons from AF and non-AF patients

A–F, example extended volume images of VACHT (green) and TH (red) immunolabelling in GP neurons from non-AF (A–C), and AF patients (D–F). G, quantification of the frequency of VACHT (left), TH (middle) and both VACHT and TH (right) positive GP neurons in non-AF ($n = 16$) and AF ($n = 8$) ganglia. GPs from AF patients showed reduced VACHT-positive neurons, increased TH-positive neurons and reduced dual phenotype neurons (Student's *t* test).

Increased electrophysiological and structural complexity of human GP neurons

Our data have identified the cellular physiological properties of human GP neurons including resting membrane potential, membrane resistance, action potential threshold and firing patterns. These data show that the discrete biophysical properties of human GP neurons are more complex than corresponding electrophysiological data we recently published from rodent GPs (Ashton et al., 2020). Specifically, in direct comparison with rodent GP neuron data from Ashton et al. (2020), human GP neurons have significantly higher capacitance reflecting increased morphological complexity (rat: 84.4 ± 29.0 vs. human: 187.1 ± 17.7 pF), lower membrane resistance likely reflecting higher density of voltage-gated membrane channels (rat: 373.8 ± 339.5 vs. human: 243.3 ± 38.5 M Ω), and faster action potential half-width (rat: 3.10 ± 0.15 ms vs. human: 1.10 ± 0.47 ms) and after-hyperpolarisation kinetics meaning a higher dynamic range of possible action potential firing rates (rat: 159.3 ± 48.8 ms vs. human: 50.8 ± 36.4 ms). Our cellular dye fills of human GP neurons also reveal significantly greater anatomical complexity of human GP neurons compared to neuronal fills from rodent GPs (Ashton et al., 2020). Unlike rodent unipolar or bipolar neurons, which have short neurite outgrowth, human GP neurons are multipolar, with significantly complex neurite branching and outgrowth. Neurites from GP neurons were observed to project to other neurons within the same ganglion or extend to other ganglia within the same plexus. This structural complexity reflects the potential for neuronal computation, communication, and dendritic summation of synaptic input in human GPs.

Physiological changes in human GP neurons occur with AF

No differences in passive membrane properties or kinetics of single action potentials were observed between GP neurons from AF vs non-AF patient tissue. However, rheobase was significantly lower in GP neurons from AF patients showing reduced current is required to reach threshold for action potential firing. In addition, the proportion of low firing GP neurons was reduced. GP neurons from AF patients therefore show a right-shifted dynamic range of action potential firing. GP neurons from AF patients were also less likely to slow their action potential firing with time (i.e. accommodate), resulting in action potential firing over a longer time period. The cause of this reduced accommodation is likely a change in K⁺ channel function altering the speed of repolarisation in GP neurons from AF patients, and/or a change in Na⁺ function resulting in lack of inactivation of the Na⁺ current altering the ability to reach threshold to fire action

potentials. Previous studies in animal models have shown that autonomic neurons that do not accommodate exhibit a prominent K⁺ current (A-type) and this increases the interspike interval, while accommodating neurons involve the M-type K⁺ current (Adams & Galvan, 1986; Cassell et al., 1986; Myers, 1998). It will be important to specifically examine both K⁺ and Na⁺ currents in human GP neurons and their role in this AF phenotype. Together these properties reveal GP neurons from AF patients are more excitable at lower levels of incoming stimulation. A potential result of this is increased activation of GP neuron target cells at lower thresholds that could contribute to aberrant activity or increased excitability that has been proposed to contribute to the substrate for AF (Lim et al., 2011; Chen et al., 2014; Salavatian et al., 2016; Carnagarin et al., 2019).

Synaptic input onto GP neurons and changes in the weighting with AF

Our data show a high density of synaptic input onto human GP neurons, highlighting potential synaptic communication occurring between networks of GP neurons. However further physiological measurements of synaptic activity will be required to confirm this. These structural synaptic sites likely reflect inputs both from the extrinsic cardiac nervous system as well as local synaptic inputs from neighbouring ganglia and GP neurons (Armour et al., 1997; Shvaley & Sosunov, 1985). This is supported by our imaging of filled GP neurons showing neurites projecting to other GP neurons within the same ganglia or out of the image area potentially to other ganglia within the same plexus.

The higher complexity of the dendritic arbors of human GP neurons compared with rodents and other mammals enables increased synaptic input to both proximal and distal dendritic branches of GP neurons. This highlights their increased structural similarity to neurons of the central nervous system. In addition, significant synaptic sites were also evident on neuronal processes wrapping around the GP neuronal somas (Fig. 1C), where we have shown glial cells to wrap around the soma (Tedoldi et al., 2021), suggesting significant synaptic input occurs onto the glial cells. The precise role of these glia is currently unknown, but their proximity to the soma and synapses suggests a role in supporting neuronal activity and plasticity as occurs in the brain (Tedoldi et al., 2021).

Quantification of synapsin1 immunostaining in GP neurons showed significantly higher synapsin1 puncta area, volume, total synapsin puncta per ganglion, as well as puncta density in AF patient tissue, consistent with greater synaptic input onto GP neurons occurring with AF. The larger presynaptic area and volume of synapsin1 suggests anatomical growth of presynaptic terminals and potential

increased presynaptic transmitter release. It will be of significant interest to determine whether the observed structural changes result in an overall increase in the strength of neurotransmission at these synapses, i.e. the expression of the major form of synaptic plasticity termed long term potentiation (Bliss & Lomo, 1973; Bliss & Collingridge 1993; Montgomery et al., 2001; Montgomery & Madison, 2002; Nicoll & Malenka 1999). Electrophysiological whole cell recordings of synaptic currents are necessary to more fully understand this. Increased synaptic input does correlate with our electrophysiological observations of lower rheobase and reduced incidence of low action potential firing frequency, as increased excitatory synaptic input will promote action potential firing.

Put together these imaging and electrophysiological observations support a lower threshold for excitability in GP neurons driving a potential substrate for AF. This also identifies the potential for opposing plasticity mechanisms that decrease synaptic excitability, e.g. long-term depression (Dudek & Bear, 1992; Montgomery & Madison, 2002), as a potential therapeutic pathway to pursue. This would include more specifically targeting decreases in neuronal ion channel conductance, increases in neuronal ion channel endocytosis, altering expression of ion channel scaffold proteins at synapses, and changes in presynaptic release probability (Castillo, 2012; Bagni & Zukin, 2019; Wang et al., 2022).

Phenotypic changes in GP neurons with AF

As well as showing a unique visual perspective of entire human GP ganglia, our large-tissue confocal imaging also revealed phenotypic differences occurring in GP neurons with AF. Specifically in GPs from AF patients we observed a lower percentage of VAcHT positive neurons, a higher percentage of TH positive neurons, and fewer dual phenotype neurons. These phenotypic changes could alter cholinergic/parasympathetic and noradrenergic/sympathetic drive to the SA node and the atria to affect autonomic balance of heart rate and rhythm regulation. High performance liquid chromatography and mass spectrometry will be needed to measure cholinergic and noradrenergic transmitter release from GP at these sites. Compelling evidence exists of imbalance between sympathetic and parasympathetic components of the autonomic nervous system contributing to AF (e.g. Chen & Tan, 2007; Czick et al., 2016; Kuyumcu et al., 2017). At this stage it is unknown whether these changes are cause or effect, i.e. do these phenotypic changes occur early and contribute to AF, or are they a resultant effect of AF. The significant decline in dual phenotype neurons suggests a loss of functional plasticity in balancing opposing inputs with AF if indeed these

neurons are capable of switching release of noradrenaline and acetylcholine (Yang et al., 2002; Furshpan et al., 1986). However immunostaining in mouse has shown the presence of TH in mouse intrinsic cardiac neurons but a lack of potential of noradrenaline storage or release (Hoard et al., 2008), so it is important to note these TH positive neurons may not release noradrenaline. Previous studies have shown additional neuronal phenotypes occur in GPs, including neuropeptides such as neuropeptide Y, neurotransmitters including dopamine and serotonin, and nitrenergic neurons positive for neuronal nitric oxide synthase (Hoover et al., 2009; Singh et al., 1999). Identifying differences in the frequency of these peptidergic, serotonergic, dopaminergic and nitrenergic neurons will be of significant interest to gauge AF-related changes in specific subtypes of GP neurons. Biochemical, imaging and electrophysiological analysis of the dual and single phenotype neurons will also be required to functionally verify which transmitters are released, and what specific activity patterns occur in GP neurons before, during and after AF, combined with *post hoc* identification of phenotype(s) described above.

In conclusion, we have provided the first description of cellular electrophysiological properties and structure of human GP neurons and how these compare in non-AF and AF patients. Our data identify the unique properties and high complexity of human GP neurons, with significant complex neurite outgrowth that more closely resemble mature neurons in the central nervous system. This represents a significant change from smaller mammals. Interestingly we observed both functional and structural differences in GP neurons from patients with AF, including increased duration of action potential firing, lower threshold of neuronal excitability, and higher synaptic input and noradrenergic phenotype. This functional and structural plasticity in the ICNS neurons may underpin AF substrate and raises opposing plasticity mechanisms as potential AF therapeutic pathways.

References

- Adams, P. R., & Galvan, M. (1986). Voltage-dependent currents of vertebrate neurons and their role in membrane excitability. *Advances in Neurology*, **44**, 137–170.
- Adke, A P., Khan, A., Ahn, H.-S., Becker, J J., Wilson, T D., Valdivia, S., Sugimura, Y K., Martinez Gonzalez, S., & Carrasquillo, Y. (2021). Cell-type specificity of neuronal excitability and morphology in the central amygdala. *eNeuro*, **8**(1), ENEURO.0402–20.2020.
- Ardell, J. L., & Armour, J A. (2016). Neurocardiology: Structure-based function. *Comprehensive Physiology*, **6**, 1635–1653.
- Armour, J. A., Murphy, D A., Yuan, B.-X., Macdonald, S., & Hopkins, D A. (1997). Gross and microscopic anatomy of the human intrinsic cardiac nervous system. *Anatomical Record*, **247**(2), 289–298.

- Armour, J. A. (2008). Potential clinical relevance of the little brain on the mammalian heart. *Experimental Physiology*, **93**(2), 165–176.
- Ashton, J L., Burton, R A. B., Bub, G., Smaill, B H., & Montgomery, J M. (2018). Synaptic plasticity in cardiac innervation and its potential role in atrial fibrillation. *Frontiers in Physiology*, **9**, 240.
- Ashton, J L., Argent, L., Smith, J E. G., Jin, S., Sands, G B., Smaill, B H., & Montgomery, J M. (2020). Evidence of structural and functional plasticity occurring within the intracardiac nervous system of spontaneously hypertensive rats. *American Journal of Physiology-Heart and Circulatory Physiology*, **318**(6), H1387–H1400.
- Bagni, C., & Zukin, R. S. (2019). A synaptic perspective of fragile X syndrome and autism spectrum disorders. *Neuron*, **101**(6), 1070–1088.
- Bliss, T. V. P., & Lomo, T. (1973). Long-lasting potentiation of synaptic transmission in the dentate area of the anaesthetized rabbit following stimulation of the perforant path. *The Journal of Physiology*, **232**(2), 331–356.
- Bliss, T. V. P., & Collingridge, G. L. (1993). A synaptic model of memory: Long-term potentiation in the hippocampus. *Nature*, **361**(6407), 31–39.
- Buckley, U., Rajendran, P S., & Shivkumar, K. (2016). Ganglionated plexus ablation for atrial fibrillation: Just because we can, does that mean we should? *Heart Rhythm*, **14**(1), 133–134.
- Cardinal, R., Pagé, P., Vermeulen, M., Ardell, J L., & Armour, J. A. (2009). Spatially divergent cardiac responses to nicotinic stimulation of ganglionated plexus neurons in the canine heart. *Autonomic Neuroscience*, **145**(1–2), 55–62.
- Carnagarin, R., Kiuchi, M G., Ho, J K., Matthews, V B., & Schlaich, M P. (2019). Sympathetic nervous system activation and its modulation: Role in atrial fibrillation. *Frontiers in Neuroscience*, **12**, 1058.
- Cassell, J. F., Clark, A. L., & McLachlan, E. M. (1986). Characteristics of phasic and tonic sympathetic ganglion cells of the guinea-pig. *The Journal of Physiology*, **372**(1), 457–483.
- Castillo, P. E. (2012). Presynaptic LTP and LTD of excitatory and inhibitory synapses. *Cold Spring Harbor perspectives in biology*, **4**(2), a005728.
- Chen, P.-S., & Tan, A Y. (2007). Autonomic nerve activity and atrial fibrillation. *Heart Rhythm*, **4**(3), S61–S64.
- Chen, P.-S., Chen, L S., Fishbein, M C., Lin, S.-F., & Nattel, S. (2014). Role of the autonomic nervous system in atrial fibrillation: Pathophysiology and therapy. *Circulation Research*, **114**(9), 1500–1515.
- Clyburn, C., Andresen, M C., Ingram, S L., & Habecker, B A. (2022). Untangling peripheral sympathetic neurocircuits. *Frontiers in Cardiovascular Medicine*, **9**, 842656.
- Clyburn, C., Li, M.-H., Ingram, S L., Andresen, M C., & Habecker, B A. (2023). Cholinergic collaterals arising from noradrenergic sympathetic neurons in mice. *The Journal of Physiology*, **601**(7), 1247–1264.
- Czick, M E., Shapter, C L., & Silverman, D I. (2016). Atrial Fibrillation: The science behind its defiance. *Aging and Disease*, **7**(5), 635–656.
- Dudek, S. M., & Bear, M. F. (1992). Homosynaptic long-term depression in area CA1 of hippocampus and effects of N-methyl-D-aspartate receptor blockade. *Proceedings of the National Academy of Sciences, USA*, **89**(10), 4363–4367.
- Edwards, F. R., Hirst, G. D., Klemm, M. F., & Steele, P. A. (1995). Different types of ganglion cell in the cardiac plexus of guinea-pigs. *The Journal of Physiology*, **486**(2), 453–471.
- Ernsberger, U., & Rohrer, H. (1999). Development of the cholinergic neurotransmitter phenotype in postganglionic sympathetic neurons. *Cell and Tissue Research*, **297**(3), 339–361.
- Furshpan, E., Landis, S., Matsumoto, S., & Potter, D. (1986). Synaptic functions in rat sympathetic neurons in microcultures. I. Secretion of norepinephrine and acetylcholine. *Journal of Neuroscience*, **6**(4), 1061–1079.
- Gibbons, D. D., Southerland, E. M., Hoover, D. B., Beaumont, E., Armour, J. A., & Ardell, J L. (2012). Neuromodulation targets intrinsic cardiac neurons to attenuate neuronally mediated atrial arrhythmias. *American Journal of Physiology*, **302**(3), R357–R364.
- Hanna, P., Dacey, M. J., Brennan, J., Moss, A., Robbins, S., Achanta, S., Biscola, N. P., Swid, M. A., Rajendran, P. S., Mori, S., Hadaya, J. E., Smith, E. H., Peirce, S. G., Chen, J., Havton, L., Cheng, Z. J., Vadigepalli, R., Schwaber, J. S., Lux, R. L., Efimov, I. R., Tompkins, J. D., Hoover, D. B., Ardell, J. L., & Shivkumar, K. (2021). Innervation and neuronal control of the mammalian sinoatrial node: A comprehensive atlas. *Circulation Research*. Published online February, **25**.
- Hoard, J. L., Hoover, D. B., Mabe, A. M., Blakely, R. D., Feng, N., & Paolocci, N. (2008). Cholinergic neurons of mouse intrinsic cardiac ganglia contain noradrenergic enzymes, norepinephrine transporters, and the neurotrophin receptors tropomyosin-related kinase A and p75. *Neuroscience*, **156**(1), 129–142.
- Hoover, D. B., Isaacs, E. R., Jacques, F., Hoard, J. L., Pagé, P., & Armour, J. A. (2009). Localization of multiple neurotransmitters in surgically derived specimens of human atrial ganglia. *Neuroscience*, **164**(3), 1170–1179.
- Horackova, M., Armour, J. A., & Byczko, Z. (1999). Distribution of intrinsic cardiac neurons in whole-mount guinea pig atria identified by multiple neurochemical coding a confocal microscope study. *Cell and Tissue Research*, **297**(3), 409–421.
- Kron, J., Kasirajan, V., Wood, M A., Kowalski, M., Han, F T., & Ellenbogen, K A. (2010). Management of recurrent atrial arrhythmias after minimally invasive surgical pulmonary vein isolation and ganglionic plexi ablation for atrial fibrillation. *Heart Rhythm*, **7**(4), 445–451.
- Kuyumcu, M. S., Ozeke, O., Cay, S., Ozcan, F., Bayraktar, M. F., Kara, M., Vicdan, M., Acar, B., Aydogdu, S., Topaloglu, S., & Aras, D. (2017). The short-term impact of the catheter ablation on noninvasive autonomic nervous system parameters in patients with paroxysmal atrial fibrillation. *Pacing and Clinical Electrophysiology*, **40**(11), 1193–1199.
- Lee, K., Park, T I.-H., Heppner, P., Schweder, P., Mee, E W., Dragunow, M., & Montgomery, J M. (2020). Human in vitro systems for examining synaptic function and plasticity in the brain. *Journal of Neurophysiology*, **123**(3), 945–965.

- Lee, K., Jung, Y., Vyas, Y., Skelton, I., Abraham, W C., Hsueh, Yi-P, & Montgomery, J M. (2022). Dietary zinc supplementation rescues fear-based learning and synaptic function in the Tbr1^{+/-} mouse model of autism spectrum disorders. *Molecular Autism*, **13**(1), 13.
- Li, W., Germain, R. N., & Gerner, M Y. (2017). Multiplex, quantitative cellular analysis in large tissue volumes with clearing-enhanced 3D microscopy (Ce3D). *Proceedings of the National Academy of Sciences, USA*, **114**, E7321–E7330.
- Lim, P. B., Malcolme-Lawes, L C., Stuber, T., Wright, I., Francis, D P, Davies, D. W, Peters, N S., & Kanagaratnam, P. (2011). Intrinsic cardiac autonomic stimulation induces pulmonary vein ectopy and triggers atrial fibrillation in humans. *Journal of Cardiovascular Electrophysiology*, **22**(6), 638–646.
- Lindh, B., & Hökfelt, T. (1990). Structural and functional aspects of acetylcholine peptide coexistence in the autonomic nervous system. *Progress in Brain Research*, **84**, 175–191.
- Linz, D., Ukena, C., Mahfoud, F., Neuberger, H.-R., & Böhm, M. (2014). Atrial autonomic innervation: A target for interventional antiarrhythmic therapy? *Journal of the American College of Cardiology*, **63**(3), 215–224.
- Mcallen, R M., Salo, L M., Paton, J F. R., & Pickering, A E. (2011). Processing of central and reflex vagal drives by rat cardiac ganglion neurones: An intracellular analysis. *The Journal of Physiology*, **589**(23), 5801–5818.
- Montgomery, J. M., Pavlidis, P., & Madison, D. V. (2001). Pair recordings reveal all-silent synaptic connections and the postsynaptic expression of long-term potentiation. *Neuron*, **29**(3), 691–701.
- Montgomery, J M., & Madison, D V. (2002). State-dependent heterogeneity in synaptic depression between pyramidal cell pairs. *Neuron*, **33**(5), 765–777.
- Myers, A. C. (1998). Ca²⁺ and K⁺ currents regulate accommodation and firing frequency in guinea pig bronchial ganglion neurons. *American Journal of Physiology*, **275**, L357–L364.
- Nicoll, R. A., & Malenka, R. C. (1999). Expression mechanisms underlying NMDA receptor-dependent long-term potentiation. *Annals of the New York Academy of Sciences*, **868**(1), 515–525.
- Park, T. I.-H., Schweder, P., Lee, K., Dieriks, B. V., Jung, Y., Smyth, L., Rustenhoven, J., Mee, E., Heppner, P., Turner, C., Curtis, M. A., Faull, R. L. M., Montgomery, J. M., & Dragunow, M. (2020). Isolation and culture of functional adult human neurons from neurosurgical brain specimens. *Brain Communications*, **2**(2), fcaa171.
- Pauza, D H., Skripka, V., Pauziene, N., & Stropus, R. (2000). Morphology, distribution, and variability of the epicardiac neural ganglionated subplexuses in the human heart. *Anatomical Record*, **259**(4), 353–382.
- Rajendran, P S., Challis, R C., Fowlkes, C C., Hanna, P., Tompkins, J D., Jordan, M C., Hiyari, S., Gabris-Weber, B A., Greenbaum, A., Chan, K Y., Deverman, B E., Münzberg, H., Ardell, J L., Salama, G., Gradinaru, V., & Shivkumar, K. (2019). Identification of peripheral neural circuits that regulate heart rate using optogenetic and viral vector strategies. *Nature Communications*, **10**(1), 1–13.
- Richardson, R. J., Grkovic, I., & Anderson, C. R. (2003). Immunohistochemical analysis of intracardiac ganglia of the rat heart. *Cell and Tissue Research*, **314**(3), 337–350.
- Rimmer, K., & Harper, A A. (2006). Developmental changes in electrophysiological properties and synaptic transmission in rat intracardiac ganglion neurons. *Journal of Neurophysiology*, **95**(6), 3543–3552.
- Salavatian, S., Beaumont, E., Longpre, J-P., Armour, JA, Vinet, A, Jacquemet, V, Shivkumar, K, & Ardell, JL (2016). Vagal stimulation targets select populations of intrinsic cardiac neurons to control neurally-induced atrial fibrillation. *American Journal of Physiology-Heart and Circulatory Physiology*, **311**(5), H1311–H1320.
- Sands, G B., Ashton, J L., Trew, M L., Baddeley, D., Walton, R D., Benoist, D., Efimov, I R., Smith, N P., Bernus, O., & Smaill, B H. (2022). It's clearly the heart! Optical transparency, cardiac tissue imaging, and computer modelling. *Progress in Biophysics and Molecular Biology*, **168**, 18–32.
- Shvaley, V. N., & Sosunov, A A. (1985). A light and electron microscopic study of cardiac ganglia in mammals. *Zeitschrift Fur Mikroskopisch-Anatomische Forschung*, **99**, 676–694.
- Singh, S., Johnson, P I., Javed, A., Gray, T S., Lonchyna, V A., & Wurster, R D. (1999). Monoamine- and histamine-synthesizing enzymes and neurotransmitters within neurons of adult human cardiac ganglia. *Circulation*, **99**(3), 411–419.
- Smith, J E. G., Ashton, J L., Argent, L P., Cheyne, J E., & Montgomery, J M. (2023). Recording plasticity in neuronal activity in the rodent intrinsic cardiac nervous system using calcium imaging techniques. *Frontiers in Synaptic Neuroscience*, **15**, 1104736.
- Tan, A Y., Zhou, S., Ogawa, M., Song, J., Chu, M., Li, H., Fishbein, M C., Lin, S.-F., Chen, L S., & Chen, P.-S. (2008). Neural mechanisms of paroxysmal atrial fibrillation and paroxysmal atrial tachycardia in ambulatory canines. *Circulation*, **118**(9), 916–925.
- Tedoldi, A., Argent, L., & Montgomery, J M. (2021). The role of the tripartite synapse in the heart: How glial cells may contribute to the physiology and pathophysiology of the intracardiac nervous system. *American Journal of Physiology-Cell Physiology*, **320**(1), C1–C14.
- Ting, J. T., Daigle, T. L., Chen, Q., & Feng, G. (2014). Acute brain slice methods for adult and aging animals: Application of targeted patch clamp analysis and optogenetics, in: *Methods in Molecular Biology*, **1183**, 221–242.
- Vyas, Y., Lee, K., Jung, Y., & Montgomery, J M. (2020). Influence of maternal zinc supplementation on the development of autism-associated behavioural and synaptic deficits in offspring Shank3-knockout mice. *Molecular Brain*, **13**(1), 110.
- Wang, X., Hayes, J A., Picardo, M C D., & Del Negro, C A. (2013). Automated cell-specific laser detection and ablation of neural circuits in neonatal brain tissue. *The Journal of Physiology*, **591**(10), 2393–2401.
- Wang, J.-H., Wu, C., Lian, Y-Na, Liu, Li, & Li, X.-Y. (2022). Targeting long-term depression of excitatory synaptic transmission for the treatment of neuropathic pain. *Federation of European Biochemical Societies Journal*, **289**(23), 7334–7342.

- Weihe, E., Schütz, B., Hartschuh, W., Anlauf, M., Schäfer, M K., & Eiden, L E. (2005). Coexpression of cholinergic and noradrenergic phenotypes in human and nonhuman autonomic nervous system. *Journal of Comparative Neurology*, **492**(3), 370–379.
- Yang, Bo, Slonimsky, J D., & Birren, S J. (2002). A rapid switch in sympathetic neurotransmitter release properties mediated by the p75 receptor. *Nature Neuroscience*, **5**(6), 539–545.

Additional information

Data availability statement

All data supporting the results in this paper are provided in the results section of the manuscript.

Competing interests

The authors hold no competing interests.

Author contributions

J.A.: performed physiology and imaging experiments, analysed data, contributed to manuscript writing. B.P.: performed imaging experiments and analysed data. G.S.: performed imaging experiments. L.A.: performed physiology and imaging experiments, contributed to manuscript writing. M.A.: responsible for patient consent and coordination of surgical team with research team. J.E.G.S.: assisted with experiments and patient samples. A.T.: performed physiology experiments, analysed data. A.A.: performed imaging experiments. D.B.: assisted with imaging experiments. A.G.P.: assisted with imaging experiments. N.L.: led clinical side of study design, provided clinical input to data interpretation, and assisted with required approvals. R.T.: cardiovascular surgeon performing epicardial adipose sampling. B.H.S.: supervised imaging component of study. J.M.M.: designed study, supervised all students and research staff, analysed data, and wrote the manuscript. All authors have read and approved the final

version of this manuscript and agree to be accountable for all aspects of the work in ensuring that questions related to the accuracy or integrity of any part of the work are appropriately investigated and resolved. All persons designated as authors qualify for authorship, and all those who qualify for authorship are listed.

Funding

This work was funded by the Royal Society New Zealand, Heart Foundation New Zealand, Marsden Fund, and the Hynds Foundation.

Acknowledgements

The authors thank members of the Cardiothoracic Surgical Unit at Auckland City Hospital for assistance with patient consent and surgical samples, tissue donors and their families. The authors also acknowledge the Centre for eResearch, University of Auckland for their assistance with data storage, and the New Zealand eScience Infrastructure (NeSI) for high-performance computing facilities.

Open access publishing facilitated by The University of Auckland, as part of the Wiley - The University of Auckland agreement via the Council of Australian University Librarians.

Keywords

atrial fibrillation, electrophysiology, ganglionated plexi, intrinsic cardiac nervous system, neurophysiology, three-dimensional tissue imaging

Supporting information

Additional supporting information can be found online in the Supporting Information section at the end of the HTML view of the article. Supporting information files available:

Peer Review History